A Nanosensor for Transmembrane Capture and Identification of Single Nucleic Acid Molecules

Jonathan Nakane,* Matthew Wiggin,[†] and Andre Marziali*

*Department of Physics and Astronomy, and [†]Department of Biochemistry, University of British Columbia, Vancouver, British Columbia, Canada

ABSTRACT   We have engineered a nanosensor for sequence-specific detection of single nucleic acid molecules across a lipid bilayer. The sensor is composed of a protein channel nanopore (α-hemolysin) housing a DNA probe with an avidin anchor at the 5′ end and a nucleotide sequence designed to noncovalently bind a specific single-stranded oligonucleotide at the 3′ end. The 3′ end of the DNA probe is driven to the opposite side of the pore by an applied electric potential, where it can specifically bind to oligonucleotides. Reversal of the applied potential withdraws the probe from the pore, dissociating it from a bound oligonucleotide. The time required for dissociation of the probe-oligonucleotide duplex under this force yields identifying characteristics of the oligonucleotide. We demonstrate transmembrane detection of individual oligonucleotides, discriminate between molecules differing by a single nucleotide, and investigate the relationship between dissociation time and hybridization energy of the probe and analyte molecules. The detection method presented in this article is a candidate for in vivo single-molecule detection and, through parallelization in a synthetic device, for genotyping and global transcription profiling from small samples.

INTRODUCTION

Heterogeneity is a fundamental feature of biological systems, yet most biochemical assays yield measurements of average values over ensembles of cells or molecules, obscuring a wealth of information about individual molecule and cell behavior. Furthermore, assays that require isolation of cellular components destroy the cells being observed and are therefore incompatible with observation of temporal dynamics of cellular processes. Although much progress has been made in understanding control networks and biochemical pathways in cells (Kitano, 2002), uncovering the temporal dynamics of such networks will necessitate time-resolved, single-cell measurement methods that can be carried out in vivo. As the operation of such networks cannot always be synchronized over a large ensemble of cells, ensemble average measurements will not be sufficient for many systems. The challenges in developing the desired assays are numerous: sufficient signal/noise ratio must be obtained, perturbations to cell function must be minimized, and a large variety of molecules must be detected with great specificity.

Although these arguments point to the need for in vivo detection and measurement techniques, near-term improvements to measurement of gene expression using DNA microarrays would also represent progress toward these goals. At present, nonspecific hybridization in microarrays results in low signal/noise ratios, even under highly stringent conditions (Schuchhardt et al., 2000). In addition, practical constraints on fluorescence detection methods used in microarrays set a lower limit on the number of molecules required for detection.

We present a first demonstration of a transmembrane single molecule sensor (Kasianowicz, 2002) with implications to a broad range of engineered transmembrane molecule detectors. By employing electronic molecule detection within a nanopore, we achieve a high signal/noise ratio and specific detection of oligonucleotides with single base resolution. Although many technical issues must be addressed to develop this sensor for in vivo applications, it has a number of advantages that make it a compelling candidate. The sensor is assembled in a lipid bilayer, and detects molecules on the side opposite to assembly, opening the possibility of assembling the sensor on the membrane of a living cell and assaying molecules in the cytoplasm. Also, unlike other in vivo detection techniques currently employed (e.g., GFP-tagging; Tsien, 1998, or lacZ-reporters; Miller, 1972), the nanosensor does not require genetic modification of the cells being observed, nor does it require introduction of foreign molecules into the cell. Development of synthetic nanopores (Li et al., 2001; Storm et al., 2003) and nanoporous membranes (Siwy and Fulinski, 2002) may allow extension of this work to the development of hybrid organic-synthetic nanosensor devices for transcript profiling or genotyping.

Our prototype nanosensor takes advantage of the geometry of the α-hemolysin (a-HL) nanopore (Song et al., 1996): the narrowest part of its aqueous channel allows passage of single-stranded DNA (ssDNA), but is impassable to double-stranded DNA (dsDNA) (Kasianowicz et al., 1996). As described in Materials and Methods, a single a-HL pore is formed in a lipid membrane, and a probe designed to bind specifically to the molecule of interest is inserted into

the pore by an applied electric potential, so that the binding region of the probe protrudes through the opposite side of the pore. Throughout the process, the ionic current is measured and monitored. A sudden step-like decrease in the current through the pore signals successful insertion of the probe. Binding of the analyte molecule to the probe traps the probe in the pore, even when the applied potential is reduced or reversed. Reversal of the potential tends to pull the probe from the pore, eventually forcing probe-analyte dissociation and allowing the probe to exit the pore, thus returning the ionic current to the open pore value. By observing kinetics of unbinding events, we are able to quantify parameters of the interaction between probe and analyte molecules.

Previous work on DNA detection in the a-HL pore has focused on analyzing the ionic current signature as DNA translocates through the pore (Kasianowicz et al., 1996, Akeson et al., 1999, Meller et al., 2001), a very difficult task given the translocation rate ($\sim$1 nt/μs at 100 mV) and the inherent noise in the ionic current signal. Higher specificity has been achieved in nanopore-based sensors by incorporation of probe molecules permanently tethered to the interior of the pore (Howorka et al., 2001a,b; Movileanu et al., 2000). However, the probe-analyte dimer must be small enough to enter the pore lumen. Similar recent work requires the probe and analyte molecules to be initially present as a duplex on one side of the membrane (Sauer-Budge et al., 2003). Other schemes require the molecule being analyzed to be of a specific shape or configuration to increase analysis times (Vercoutere et al., 2001, 2003).

Our sensor differs from previous approaches in several important details: limitations from translocation rate are avoided in this work since detection is based on the presence or absence of the probe strand inside of the pore, with a signal/noise ratio >50. The probe molecule extends across the membrane to access target molecules on the opposite side, allowing for true trans-membrane detection. The probe is also separate from the pore, allowing for easy modifications in probe design with unmodified biological or synthetic pores; the analyte molecule does not translocate through the pore, allowing the analyte-probe duplex to be larger than the pore. The probe in our sensor is uniformly charged, yielding greater control over the dissociation force and giving greater access to information on the energetics of interaction between probe and analyte.

Unlike the vast majority of biochemical assays that are colorimetric, fluorescent, or chemiluminescent, nanopore detection only requires electrical measurement of ionic current through the pore, and requires no optics or fluorescent labels. The ability to detect single unmodified analytes makes the nanosensor less likely to interfere with cell function by depleting or altering analytes, making it an excellent candidate for in vivo measurement. With further adaptation of probes, it may be possible to assay specific protein or other biomolecule levels by incorporating sequences for RNA aptamers into the probes. Although many challenges need to be overcome for eventual in vivo application of this sensor, it should be noted that single channel recordings have been successfully taken from α-hemolysin incorporated into Lettre cells (Korchev et al., 1995). The general technique we describe may also be amenable to in vitro applications such as genotyping or transcription profiling with availability of suitable nanopore membranes.

MATERIALS AND METHODS

The sensor is constructed in vitro using a method modified from that of Akeson and co-workers (Akeson et al., 1999; Nakane et al., 2003; see also Fig. 1, this article). A lipid bilayer is formed across a $\sim$50-μm hole in a Teflon tube which connects two reservoirs. The reservoirs and Teflon tube are filled with microfiltered buffered 1 M KCl (10 mM HEPES, 1 mM EDTA, pH 8.0) as the conducting medium. Each reservoir contains a silver chloride-coated electrode from a patch-clamp amplifier (Axopatch 200B, Axon Instruments, Foster City, CA). Data acquisition software and hardware (Labview, National Instruments, Austin, TX) is used to record the applied electric potential and ionic current data from the experiment and to apply various electric potential profiles across the pore. All data is low-pass filtered at 10 kHz and digitized at 50 kHz for analysis. The pore is formed by addition of monomeric α-hemolysin (CalBioChem, San Diego, CA) to one side of the bilayer (the cis side). Pore formation is detected by applying a 100-mV electric potential across the bilayer with the anode on the trans side of the membrane, and waiting for a stepwise increase in the measured current from 0 pA to $\sim$100 pA. The cis chamber is then rinsed with fresh buffer solution to prevent formation of other pores. Under these conditions, the open pore shows a forward resistance of $\sim$1 GΩ. For tests of the sensor, 14-mer single-stranded DNA analyte (MWG Biotech, High Point, NC) was added to the solution on the trans side of the pore before bilayer formation at 2 μM.

The probe molecule is constructed from a 65-mer, ssDNA molecule, biotinylated at its 5'end (MWG Biotech, High Point, NC), with the 14 nucleotides at the 3' end forming the active portion of the probe: 5'-(A_{51})CCAAACCAACCACC-3'. To prevent probes from translocating through the pore, avidin (Molecular Probes, Eugene OR) is hybridized to the biotin, to form a large molecular anchor that is excluded from the pore. The probe molecule is added to the cis side of the pore at a concentration of 10 μM. Application of a +200 mV forward potential (anode on trans side) across the bilayer induces the free end of a probe molecule to enter the pore and translocate to the trans side until held in place by the avidin anchor. The
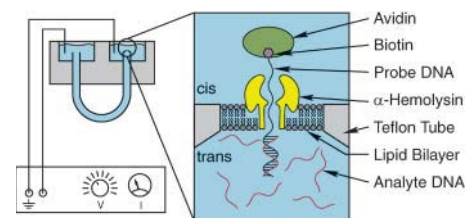

FIGURE 1 Nanosensor schematic (not to scale). An α-hemolysin nanopore is self-assembled in a lipid bilayer formed across a $\sim$50-μm opening in a Teflon tube. The tube, and the baths it opens onto are filled with 1 M KCl pH 8.0. The potential across the bilayer is controlled by an Axopatch 200B patch-clamp amplifier through AgCl electrodes. The biotinylated 5' end of the probe is bound to avidin on the cis side, preventing the probe from passing through the pore. A 14-nucleotide sequence at the 3' end of the probe is selected to hybridize to the analyte molecule, shown associated with the probe.

presence of probe in the pore restricts flow of other ions, increasing the resistance of the pore to ~4 GΩ. The probe is held in this position (~1 s) to allow time for an analyte molecule to hybridize to the probe on the *trans* side of the pore. To determine whether analyte is bound to the probe, we lower the potential across the bilayer to +10 mV. At this potential, unbound probes tend to quickly exit the pore, resulting in a return to a low-resistance state (~1 GΩ). This step is performed only to avoid collecting data on events that do not result in analyte capture. Although some unbound probes remain in the pore beyond the duration of the 10-mV hold time, this results in very short-lived events that do not contribute to the average event lifetime as calculated based on dominant timescales. Accumulation of statistics on the number of probe escapes during the 10-mV hold can yield information on analyte concentration, although this is not pursued in this article.

Probes bound to analyte molecules, however, remain trapped in the pore by the probe-analyte duplex. The applied potential is then reversed (anode on *cis* side) to ~−30 mV to −90 mV, which adds a force tending to separate the probe from the analyte and withdraw the former from the pore. In the reversed state, the blocked channel impedance is 4–10 GΩ whereas the open channel impedance is 1.5 GΩ. With continued application of this potential, the bonds forming the analyte-probe duplex eventually dissociate, allowing the probe to escape and returning the pore to a low impedance state.

The analyte molecules used in the study consisted of fully complementary 14-mer oligonucleotides and various other strands with single nucleotide mismatches within the sequence as shown in Table 1.

Using the technique outlined in Fig. 2, single molecule binding and unbinding is monitored by observing the electrical impedance of the pore to determine whether the probe molecule is present. The electric potential applied across the pore results in an electrostatic force that acts on the probe. Variation of this potential allows us to measure the dependence of the analyte-probe bond survival time on applied force.

RESULTS AND DISCUSSION

The dependence of the analyte-probe duplex lifetime on applied force can be used to uncover both the binding energy of the duplex and the width of the energy barrier in the direction of the force. The bond lifetime t_{off} is modeled from an Arrhenius relationship for escape over an energy barrier, with the barrier height discounted by the applied force projected in the direction of the reaction coordinate (Evans, 2001), which in this case is assumed to be the direction of the pore axis:

$$t_{off} = t_{D}e^{(E_{b}/kT)}e^{(-f/f_{b})}. \tag{1}$$

The value t_{D} is a diffusive relaxation time associated with the duplex, E_{b} is the height of the energy barrier, f is the applied force, and f_{b} is the thermal force scale defined as $f_{b} = kT/\Delta x_{barrier}$. $\Delta x_{barrier}$ is the energy barrier width and thus re-

lated to the distance by which the molecules must be separated along the reaction coordinate for dissociation to occur. Repeated measurements of t_{off} for the same molecule under different applied forces f (controlled by the applied reverse potential) will yield details of the dominant free energy barrier in the analyte-probe bond energy landscape in one dimension along the pore axis. For large values of f, it is possible that outer barriers will be sufficiently lowered to uncover inner barriers (Evans, 2001).

Probe-pore interaction

Before applying the sensor to oligonucleotide detection, it was necessary to calibrate it by measuring the applied potential that corresponds to zero force applied to the probe-analyte duplex. The free energy cost associated with confinement of the probe adds an entropic recoil force (Turner et al., 2002), so that at zero applied potential we expect a net force tending to remove the probe from the pore. To estimate this entropic recoil force we measured the probe escape time as a function of applied potential without analyte molecules present. We captured the probe at +200 mV, decreased the potential to a small preset forward voltage, and measured the time to probe escape. The mean escape time for each voltage tested is shown in Fig. 3.

A plot of mean time to probe escape under small forward potentials shows two distinct regimes, suggesting the presence of a transition at $V_{t} = 10.3$ mV from diffusion-limited escape, to escape over a free energy barrier. The exponential fit to the barrier-crossing region takes the form $t = (9.5 \ \mu s)*e^{0.8151*V}$, where V is the applied potential in mV. This is expected from the Arrhenius form for the time to cross a free-energy barrier, $t = t_{D}e^{(U_{0}+\Delta U)/k_{b}T}$, where ΔU is the increment in the barrier height resulting from the applied potential, and U_{0} is the entropic cost of confining the probe to the pore. Of the 65 nucleotides composing the probe, we estimate from a-HL dimensions (Song et al., 1996) that ~40 are on the *trans* side of the membrane, whereas 12 are located in the narrow region of the pore, across which the majority of the electric potential falls (Meller et al.). A first approximation of the energy barrier height increment is $\Delta U/k_{b}T = (40 + 12/2)z(e/k_{b}T)V$, where z is the fractional average charge per nucleotide, and $e/k_{b}T$ is ~$(25$ mV$)^{-1}$ at 20°C. Comparing this to the measured exponent 0.815 mV^{-1}

TABLE 1   Sequences and binding energies of molecules used in this study

Molecule	Sequence	Binding energy to probe	
Probe	3′ CCACCAACCAAACC(A$_{51}$)5′-biotin		
14-pc	5′-GGTGGTTGGTTTGG-3′	−22 kcal/mol	−37.7 $k_{b}T$ @ 20°C
14-7C	5′-GGTGGTT**C**GTTTGG-3′	−16 kcal/mol	−27.4 $k_{b}T$ @ 20°C
14-10C	5′-GGTG**C**TTGGTTTGG-3′	−15.8 kcal/mol	−27.1 $k_{b}T$ @ 20°C
14-1A	5′-GGTG**G**TTGGTTTG**A**-3′	−21.5 kcal/mol	−36.9 $k_{b}T$ @ 20°C

Binding energies were calculated using an empirical algorithm on the Mfold DNA hybridization server (Zuker, 2003). Calculations were carried out at 20°C assuming 1 M NaCl. Underlined letters indicate the mismatched basepairs in the target sequences.
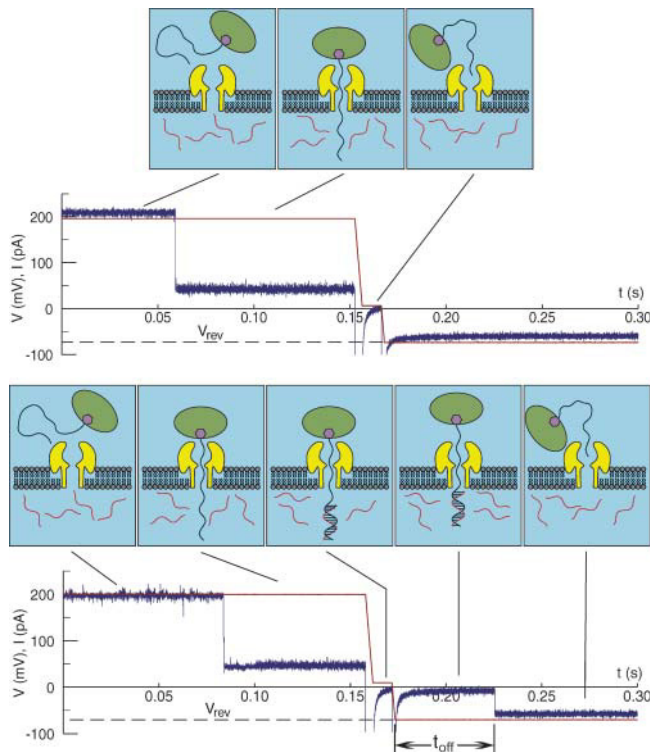
FIGURE 2 (*Upper*) Animation and experimental data of an unsuccessful
analyte capture. Current is shown in blue; applied potential is shown in red.
A +200 mV forward potential is used to capture a probe in the pore; probe
capture is observable as a decrease in current to ~25% of the open channel
value corresponding to a pore resistance increase from 1 GΩ to 4 GΩ. The
potential is then reduced to +10 mV, a potential insufficient to prevent probe
exit, and impedance returns to the open channel value. Large current spikes
during potential changes are due to capacitance of the lipid bilayer and
patch-clamp electronics. (*Lower*) Animation and experimental data of
a successful analyte capture. After probe capture, the potential is again
reduced to +10 mV for a short period, but probe exit is now prevented by the
bound analyte, and impedance remains at the blocked channel value. The
potential is then reversed to −60 mV thus applying a force to withdraw the
probe from the pore. After a time t_{off} the probe dissociates from the analyte
and the open channel (reverse) current is restored. Statistical analysis of
many dissociation events lifetimes (t_{off}) at several reverse potentials (V_{rev})
yields identifying characteristics of the analyte molecule.

and assuming that $\Delta U = -U_0$ at $V_t = 10.3$ mV, yields the
values $z = 0.4$, $t_D \sim 3$ ns, and $U_0 \sim 8\,k_bT$ for the free energy
cost of confining the probe to the pore, which is in close
agreement with other experimental estimates (Henrickson
et al., 2000). Considering that at $V_t \sim 10$ mV the free energy
cost of probe confinement and the electrostatic energy gain
of probe escape are balanced, we use this potential as a base-
line for the effective force applied to the probe-analyte bond.

Detection and identification of oligonucleotides differing by a single nucleotide

To test the sensor's ability to detect and distinguish
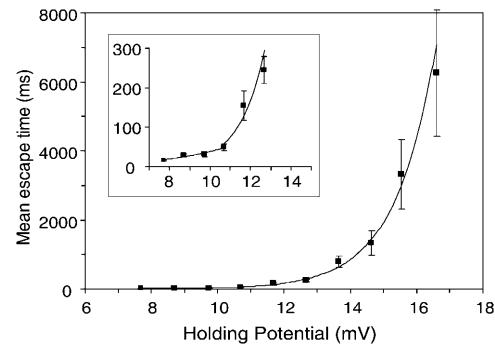oligonucleotides, we exposed it to solutions of the analytes

FIGURE 3   Mean time for the probe molecule to escape from the pore to
the *cis* chamber, under small forward applied potentials. Each data point
represents the mean of ~60 escape events. The lines drawn through the data
points represent exponential fits to points above and below 10.5 mV. The
transition from a diffusion-limited to an exponential barrier-crossing be-
havior (*inset*) occurs at a threshold potential $V_t = 10.3$ mV, calculated from
the intersection of exponential fits to the data above and below 10.5 mV.
Based on previous work (Meller et al., 2001) we expect escape time in the
diffusion-limited regime to have a quadratic relationship to potential,
although not enough data points were collected to confirm this. For each
potential, two distinct timescales for probe escape are observed as noted in
previous work (Bates et al., 2003). Although timescales for escape observed
for a 60-mer oligonucleotide by Bates et al. are substantially shorter (165 μs
and 3.5 ms) than those observed here, the former were recorded for
oligonucleotides without bound avidin, and with no applied potential to
counteract entropic recoil. At +10.5 mV applied potential, we observe the
timescales of 1.5 ms and 120 ms.

listed in Table 1 and recorded the binding event charac-
teristics associated with each solution to see whether the
characteristics of the fully complementary sequence (14pc)
were distinguishable from oligonucleotides that differed
from this sequence by a single nucleotide. We assembled the
sensor as previously described with probe molecules on the
cis side of the membrane and analyte molecules on the *trans*
side. Typical experimental measurements of unsuccessful
and successful analyte captures are shown in Fig. 2.

Fig. 4 shows the cumulative distribution of event lifetimes
for the 7c analyte at −55 mV, representing the probability
$P_{esc}(t)$ that the event will end (resulting in escape of the
probe), within a given time. We used a non-negative least-
squares error fit with regularization (Whitall and MacKay,
1989) on a multiexponential expansion of P_{esc} to find the
dominant timescales for each molecule and potential, with
P_{esc} taking the form

$$P_{esc}(t) = 1 - \sum_i a_i e^{-t/t_i}, \qquad (2)$$

and time constants ranging from 20 μs to 20 s:
$t_i = (10^{0.125i}/50{,}000)\,s;\ i = 0 - 48$. The function mini-
mized for the fit is

$$\sum \left[1 - P_{esc}(t) - \sum_i a_i e^{t/t_i} \right]^2 + 0.1 \sum_i a_i, \qquad (3)$$

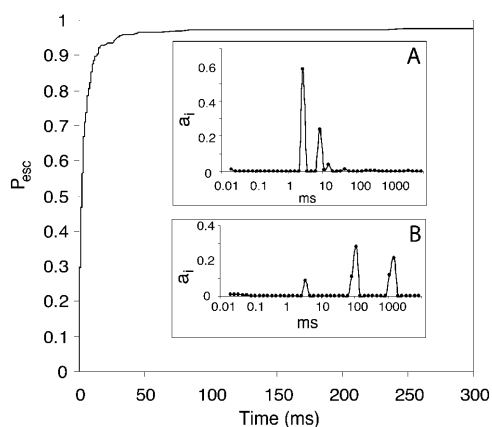where a_i represents the free parameters.

FIGURE 4 Probability of probe escape (P_{esc}) as a function of time for probe bound to the 7c molecule at −55mV potential. The data in the figure represent 417 binding events. Inset a shows the result of a non-negative least-square error fit to P_{esc} assuming the form $P_{esc} = 1 - \sum_i a_i e^{-t/t_i}$. The amplitude of the coefficients a_i is plotted on the vertical axis, whereas the timescales t_i used in the fit are plotted on the horizontal axis. For the 7c molecule data shown in this figure, the dominant timescales are 2.7 ms (with $a_i = 0.58$) and 8.4 ms ($a_i = 0.24$). Inset b shows a similar fit obtained on the P_{esc} data for the 14pc molecule at −55 mV. Dominant timescales are 100 ms ($a_i = 0.39$) and 1.3 s ($a_i = 0.34$).

FIGURE 5 Average measured event lifetimes extracted from non-negative least-square error fits to $P_{esc}(t)$. Each data point shown in the graph is a coefficient-weighted average of the dominant timescales. Any spurious and poorly resolved short- and long-lived timescales were omitted from the average. The inset shows the timescales for the 10c molecule, with the diameter of the data points representing the relative amplitude of the coefficients. The dotted line separates the dominant timescales included in the average, and the excluded spurious short-lived timescales. Lines drawn through the data in the main graph represent exponential fits, although the rightmost two points for the 10c molecule were not included in the fit (see text). For all molecules, the average event duration decreases with increasing reverse potential. Each data point represents from 60 to 500 successful analyte captures. Error bars for two of the 14pc points have been omitted for clarity: they are +4.2 ms, −2.7 ms at −75 mV; and +3.6 ms, −2.0 ms at −80 mV. Errors bars were calculated by applying a bootstrap algorithm to the collected data to get estimates for all the coefficients a_i, with each peak in the coefficient graph then fit to a Gaussian curve to estimate the mean and standard error of each peak; the composite error bars were found by adding the errors in the combined timescales in quadrature.

Inset a to Fig. 4 shows the result of this fit for the adjoining data; inset b shows the fit to $P_{esc}(t)$ for the 14pc molecule at −55 mV. Typically $P_{esc}(t)$ seems to be dominated by one or two timescales, presumably representing the unbinding kinetics of the analyte-probe duplex, although poorly defined shorter and longer timescales appear in most of the data.

Although the multiplicity of timescales appearing in the data may suggest multiple processes for probe escape after analyte binding, the identification of these processes will require additional data and is beyond the scope of this article. We assume for now that the dominant process required for probe escape is unbinding of the probe-analyte duplex. Analyte molecules incorrectly hybridized to the probe may contribute to short timescale events, as do the occasional delayed escapes of unbound probe molecules. Occasional long-lived events may result from the probe or probe-analyte duplex becoming lodged in the pore leading to blockages lasting seconds to minutes, as previously observed in studies of ssDNA translocation through the a-HL pore (Kasianowicz et al., 1996).

Averaged dominant timescales for the molecules in Table 1 are plotted as a function of the applied potential in Fig. 5.

The average characteristic lifetime for each reverse potential was obtained as $t_{avg} = \exp[\sum_j a_j \ln(t_j)/\sum_j a_j]$, where j is the set of coefficients pertaining to dominant timescales. Spurious, poorly resolved long and short-lived timescales with small amplitudes of the coefficient are not counted in this average under the assumption that they belong to events un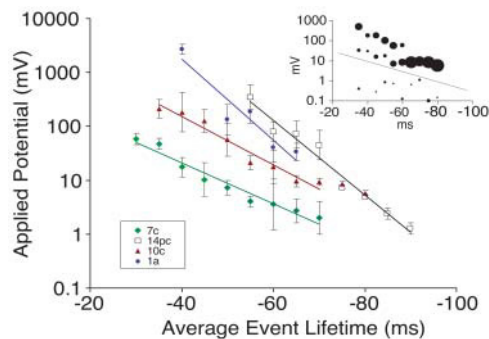related to probe-analyte dissociation as described above. An example of selection of timescales for this average is shown in the inset of Fig. 5. Each point in this plot represents a timescale for the 10c molecule, with the diameter of the circle indicating the relative amplitude of the coefficient. All points below the dotted line are rejected; those above the dotted line are included in the average.

Analyte molecules differing in sequence by a single nucleotide yield measurably different binding event lifetime versus potential characteristics, and can be discriminated using this sensor if enough events are detected. Lifetimes decrease exponentially with applied potential as expected, and, in general, are shorter for the molecules that are not perfectly matched to the probe. These lifetime trends are supported by earlier unzipping experiments using nanopores with much longer complementary regions (50 nt) and much larger mutations (four mismatches) (Sauer-Budge et al., 2003). The lifetime versus potential curve for the 10c molecule near 80 mV deviates from a simple exponential relationship. This may indicate that multiple energy barriers are associated with unbinding of 10c from the probe, and that near 80 mV the outer barrier has been lowered below an inner barrier, changing the slope of the lifetime-potential relation beyond that point.

The natural logarithm of the expected event lifetime from Eq. 1 is

$$\ln(t_{\text{off}}) = \left(\frac{-zN\Delta x}{\Delta l(25\,\text{mV})}\right)V + \frac{E_{\text{b}}}{k_{\text{b}}T} + \ln(t_{\text{D}}), \qquad (4)$$

where the electrostatic force has been approximated as zN eV/Δl, the effective charge per nucleotide is z, and there are N nucleotides present in the region over which the potential drop occurs (Δl).

The slope of the lifetime versus potential relationship for each molecule is proportional to the width of the energy barrier for probe escape projected along the reaction coordinate, with steeper slope implying a wider barrier (Evans, 2001). Assuming that each nucleotide of the probe strand is separated by ~0.5 nm, $N/\Delta l = 2$ nm^{-1} and the slope is $z\Delta x/12.5$ mV^{-1}. We propose that fracture of the duplex occurs as cooperative unbinding of N bonds in series (Strunz et al., 1999); the width of the energy barrier Δx then corresponds to Nx_{b}, where x_{b} is the width of the individual bond barriers and the distance traveled by the probe with each bond dissociation. Using our estimate of $z = 0.4$ we find Δx ~4–6 nm for 14pc and 1a, and x_{b} ~0.35 nm. Given a duplex base separation of 0.32 nm and a ssDNA base separation of 0.5 nm, we expect x_{b} ~0.2 nm. Previous studies of short DNA duplex dissociation under force (Strunz et al., 1999) yield smaller values (~0.12 nm), although under different conditions.

For the 10c and 7c molecules, the calculated energy barrier widths are Δx ~1.5–4 nm. This is possibly a result of the fact that 7c and 10c contain two shorter regions of complementary sequence, whereas 14pc and 1a have a single contiguous region of complementary sequence. It is plausible, particularly given the high reverse potential behavior seen in the 10c data, that fitting a single exponential to the lifetime-potential curve of the 7c and 10c molecules over the entire measurement range obscures details of the energy barrier.

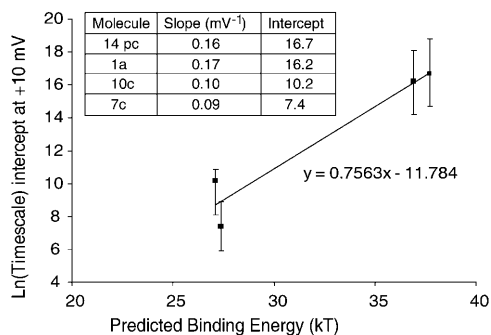| Molecule	Slope (mV^{-1})	Intercept
14 pc	0.16	16.7
1a	0.17	16.2
10c	0.10	10.2
7c	0.09	7.4

$y = 0.7563x - 11.784$

FIGURE 6   Intercept (at $V = +10$ mV) of the natural logarithm of the average event lifetime versus applied potential, plotted against the expected binding energy for each molecule, calculated from Mfold (Zuker, 2003). The intercept (at zero effective applied force) of the logarithm of the bond lifetime, as given in Eq. 4, is $(E_{\text{b}}/k_{\text{b}}T) + \ln(t_{\text{D}})$. Plotting this against the molecule binding energy in units of $k_{\text{b}}T$ as predicted by Mfold is expected to yield a linear relationship with a slope of 1. A linear fit through the data yields a slope of 0.75 +38, −0.3.

The relationship between the intercepts of the curves in Fig. 5 and the binding energies expected from Mfold (Zuker, 2003) calculations is shown in Fig. 6. Based on our estimates of the applied potential necessary to compensate for the free energy of probe confinement, intercepts are calculated at a forward potential of +10 mV, where $\Delta U = 0$. Based on Eq. 4, the relationship between these intercept values and binding energies in units of $k_{\text{b}}T$ (at 20°C) should yield a slope of 1 with an intercept of $\ln(t_{\text{D}})$. The slope obtained from this plot is 0.75 +0.38, −0.3, and the large uncertainty in the intercept values precludes any useful estimate of t_{D}.

CONCLUSIONS

We have demonstrated a proof-of-concept for a single molecule oligonucleotide sensor capable of distinguishing short oligonucleotides with single basepair resolution. The trans-membrane operation of the sensor makes it a tantalizing candidate for limited in vivo applications in cell types that are susceptible to a-HL insertion, as well as an exciting candidate for a new class of in vitro DNA sensors. Although the most likely application of this sensor would see many such sensors working in parallel, the highly accurate temporal control that can be exerted over this sensor should allow synchronization of many sensors, and the same data described in this article could be collected in a single multi-molecule event. Although this would appear to obviate the need for single molecule detection, it should be noted that such operation is fundamentally different from asynchronous measurements over an ensemble of molecules.

The data collected in this initial demonstration contains many details that have not been addressed in this manuscript. In particular, the multiple timescales for the binding event duration (that manifest themselves in the escape probability of the probe) hint at the possibility of multiple processes for unbinding of the probe-analyte duplex and escape of the probe. Investigation of these processes and their biophysical implications is an exciting priority for future work, and a stepping stone to redesign of the probe to reduce the number of timescales for probe escape—thereby increasing the likelihood that the sensor will be successful at distinguishing oligonucleotides that are present in mixes of other molecules.

REFERENCES

Akeson, M., D. Branton, J. J. Kasianowicz, E. Brandin, and D. W. Deamer. 1999. Microsecond timescale discrimination among polycytidylic acid, polyadenylic acid, and polyuridylic acid as homopolymers or as segments within single RNA molecules. *Biophys. J.* 77:3227–3233.

Bates, M., M. Burns, and A. Meller. 2003. Dynamics of DNA molecules in a membrane channel probed by active control techniques. *Biophys. J.* 84:2366–2372.

Evans, E. 2001. Probing the relation between force lifetime and chemistry in single molecular bonds. *Annu. Rev. Biophys. Biomol. Struct.* 30:105–128.

Henrickson, S. E., M. Misakian, B. Robertson, and J. J. Kasianowicz. 2000. Driven DNA transport into an asymmetric nanometer-scale pore. *Phys. Rev. Lett.* 85:3057–3060.

Howorka, S., S. Cheley, and H. Bayley. 2001a. Sequence-specific detection of individual DNA strands using engineered nanopores. *Nat. Biotechnol.* 19:636–639.

Howorka, S., L. Movileanu, O. Braha, and H. Bayley. 2001b. Kinetics of duplex formation for individual DNA strands within a single protein nanopore. *Proc. Natl. Acad. Sci. USA.* 98:12996–13001.

Kasianowicz, J. J. 2002. Nanometer-scale pores: potential applications for analyte detection and DNA characterization. *Dis. Markers.* 18:185–191.

Kasianowicz, J. J., E. Brandin, D. Branton, and D. W. Deamer. 1996. Nanometer-scale pores: potential applications for analyte detection and DNA characterization. *Proc. Natl. Acad. Sci. USA.* 93:13770–13773.

Kitano, H. 2002. Systems biology: a brief overview. *Science.* 295:1662–1664.

Korchev, Y. E., G. M. Alder, A. Bakhramov, C. L. Bashford, B. S. Joomun, E. V. Sviderskaya, P. N. R. Usherwood, and C. A. Pasternak. 1995. *Staphylococcus aureus* α-toxin-induced pores: channel-like behavior in lipid bilayers and patch-clamped cells. *J. Membr. Biol.* 143:143–151.

Li, J., D. Stein, C. McMullan, D. Branton, M. J. Aziz, and J. A. Golovchenko. 2001. Ion-beam sculpting at nanometre length scales. *Nature.* 412:166–169.

Meller, A., L. Nivon, and D. Branton. 2001. Voltage-driven DNA translocations through a nanopore. *Phys. Rev. Lett.* 86:3435–3438.

Miller, J. H. 1972. Experiments in Molecular Genetics. Cold Spring Harbor Laboratory, Cold Spring Harbor, NY.

Movileanu, L., S. Howorka, O. Braha, and H. Bayley. 2000. Detecting protein analytes that modulate transmembrane movement of a polymer chain within a single protein pore. *Nat. Biotechnol.* 18:1091–1095.

Nakane, J. J., M. Akeson, and A. Marziali. 2003. Evaluation of nanopores as candidates for electronic analyte detection. *J. Phys. Cond. Mat.* 15:R1365–R1393.

Sauer-Budge, A. F., J. A. Nyamwanda, D. K. Lubensky, and D. Branton. 2003. Unzipping kinetics of double-stranded DNA in a nanopore. *Phys. Rev. Lett.* 90:23810.

Schuchhardt, J., D. Beule, A. Malik, E. Wolski, H. Eickhoff, H. Lehrach, and H. Herzel. 2000. Normalization strategies for cDNA microarrays. *Nucleic Acids Res.* 28:e47i–e47v.

Siwy, Z., and A. Fulinski. 2002. Fabrication of a synthetic nanopore ion pump. *Phys. Rev. Lett.* 89:198103.

Song, L. Z., M. R. Hobaugh, C. Shustak, S. Cheley, H. Bayley, and J. E. Gouaux. 1996. Structure of staphylococcal α-hemolysin, a heptameric transmembrane pore. *Science.* 274:1859–1866.

Storm, A. J., J. H. Chen, X. S. Ling, H. W. Zandbergen, and C. Dekker. 2003. Fabrication of solid-state nanopores with single-nanometre precision. *Nature Mat.* 2:537–540.

Strunz, T., K. Oroszlan, R. Schafer, and H. Guntherodt. 1999. Dynamic force spectroscopy of single DNA molecules. *Proc. Natl. Acad. Sci. USA.* 96:11277–11282.

Tsien, R. Y. 1998. The green fluorescent protein. *Annu. Rev. Biochem.* 67:509–544.

Turner, S. W. P., M. Cabodi, and H. G. Craighead. 2002. Confinement-induced entropic recoil of single DNA molecules in a nanofluidic structure. *Phys. Rev. Lett.* 88:128103.

Vercoutere, W., S. Winters-Hilt, H. Olsen, D. Deamer, D. Haussler, and M. Akeson. 2001. Rapid discrimination among individual DNA hairpin molecules at single-nucleotide resolution using an ion channel. *Nat. Biotechnol.* 19:248–252.

Vercoutere, W. A., S. Winters-Hilt, V. De Guzman, D. Deamer, S. E. Ridino, J. T. Rodgers, H. E. Olsen, A. Marziali, and M. Akeson. 2003. Discrimination among individual Watson-Crick base pairs at the termini of single DNA hairpin molecules. *Nucleic Acids Res.* 31:1311–1318.

Whitall, K. P., and A. L. MacKay. 1989. Quantitative interpretation of NMR relaxation data. *J. Magn. Reson.* 84:134–152.

Zuker, M. 2003. Mfold web server for nucleic acid folding and hybridization prediction. *Nucleic Acids Res.* 31:3406–3415.